

Article

## Retrieval of Land Surface Temperature over the Heihe River Basin Using HJ-1B Thermal Infrared Data

Xiaoying Ouyang<sup>1</sup> \*, Li Jia<sup>1,2</sup>, Yingqi Pan<sup>1</sup> and Guangcheng Hu<sup>1</sup>

<sup>1</sup> State Key Laboratory of Remote Sensing Science, Institute of Remote Sensing and Digital Earth, Chinese Academy of Sciences, Beijing 100101, China; E-Mails: jiali@radi.ac.cn (L.J.); panyq@radi.ac.cn (Y.P.); hugc@radi.ac.cn (G.H.)

<sup>2</sup> Joint Center for Global Change Studies, Beijing 100875, China

\* Author to whom correspondence should be addressed; E-Mail: ouyangxy@radi.ac.cn; Tel.: +86-135-2279-2960; Fax: +86-10-6480-7983.

Academic Editors: George P. Petropoulos and Prasad S. Thenkabail

Received: 20 August 2014 / Accepted: 23 December 2014 / Published: 29 December 2014

---

**Abstract:** The reliable estimation of spatially distributed Land Surface Temperature (LST) is useful for monitoring regional land surface heat fluxes. A single-channel method is developed to derive the LST over the Heihe River Basin in China using data from the infrared sensor (IRS) onboard the Chinese “Environmental and Disaster Monitoring and Forecasting with a Small Satellite Constellation” (HJ-1B for short for one of the satellites), with ancillary water vapor information from Moderate Resolution Imaging Spectroradiometer (MODIS) products (MOD05) and *in situ* automatic sun tracking photometer CE318 data for the first time. *In situ* LST data for the period from mid-June to mid-September 2012 were acquired from automatic meteorological stations (AMS) that are part of Heihe Watershed Allied Telemetry Experimental Research (HiWATER) project. MOD05-based LST and CE318-based LST are compared with *in situ* measurements at 16 AMS sites with land cover types of vegetable, maize and orchards. The results show that the use of the MOD05 product could achieve a comparable accuracy in LST retrieval with that achieved using the CE318 data. The largest difference between the MOD05-based LST and CE318-based LST is 0.84 K throughout the study period over the Heihe River Basin. The standard deviation (STD), root mean square error (RMSE), and correlation coefficient (R) of HJ-1B/IRS vs. the *in situ* measurements are 2.45 K, 2.78 K, and 0.67, respectively, whereas those for the MODIS 1 km LST product vs. the *in situ* measurements are 4.07 K, 2.98 K, and 0.79, respectively. The spatial pattern of the HJ-1B/LST over the study area

in the Heihe River Basin generally agreed well with the MODIS 1 km LST product and contained more detailed spatial textures.

**Keywords:** land surface temperature; HJ-1B; Heihe River Basin; single-channel algorithm

---

## 1. Introduction

Land Surface Temperature (LST), one of the most important key parameters in the water balance and energy exchange between the surface and atmosphere, is widely used in many applications [1–4]. To obtain spatial and temporal records of LST, retrievals from satellite observations, such as geostationary and polar-orbit satellites, are of fundamental importance in global and regional studies [5,6]. Due to technical constraints, it is difficult to acquire remotely sensed LST with high spatial, temporal and spectral resolutions simultaneously from a single sensor. For example, although the new Landsat 8 Thermal Infrared Sensor (TIRS) provides two thermal infrared bands, the revisit frequency of 16 days makes it difficult to apply in environmental studies that require more frequent information [6]. Low spectral information, which usually has only one thermal band for sensors with high spatial resolution, impedes the accurate atmospheric correction of satellite data because single-channel sensors observe much less information on atmospheric conditions than multi-channel sensors [7–10].

The Chinese “Environmental and Disaster Monitoring and Forecasting with a Small Satellite Constellation” (HJ-1B for short for one of the satellites) have been widely used in various studies [11,12], including those that use agricultural production analyses, vegetation indexes and evapotranspiration estimates. In addition, HJ-1B satellite could also be used in Urban Heat Island (UHI) studies and fragile ecosystem studies due to its relatively high temporal frequency and high spatial resolution, which can provide global coverage every two days with a spatial resolution of 300 m. However, the HJ-1B satellite has only one infrared sensor (IRS), and only single-channel methods can be used in LST estimation.

Many studies of single-channel methods have been published. To solve the atmospheric correction problems associated with single-channel sensors, Qin and Karnieli [7] developed a mono-window algorithm for LST retrieval from Landsat TM6 data. Jiménez-Muñoz and Sobrino [13] developed a generalized single-channel method and applied to the Landsat Thematic Mapper (TM) for LST retrieval via Water Vapor Content (WVC) rather than atmospheric vertical profiles of air temperature and relative humidity obtained by radiosonde. Sobrino and Jiménez-Muñoz [14] also noted that the single-channel method provides similar or better results than the split-window for low atmospheric WVC conditions. The accuracy of atmospheric WVC is crucial because of its large impacts on atmospheric downwelling and upwelling radiances. Li [15] developed a single-channel algorithm based on a parametric model, which is more suitable for HJ-1B/IRS due to its better accuracy. Zhao *et al.* [16] performed an error analysis of LST retrieval from HJ-1B/IRS data and confirmed that the LST retrieved from HJ-1B/IRS could not be higher than 1 K unless accurate atmospheric profile and land surface emissivity (LSE) data were applied. Coll *et al.* [17] used different sources of atmospheric profiles to retrieve LST with the single-channel method, and the result indicated that the retrieved LSTs based on radiosonde atmospheric profiles were better than that based on re-analysis profiles and satellite sounder products. Yet it is still difficult

to obtain radiosonde data routinely. Zhou *et al.* [18] improved a mono-window method for HJ-1B/IRS retrievals by considering the viewing zenith angle, yielding an accuracy better than 1 K.

Although studies have been performed on HJ-1B LST retrieval, further studies of HJ-1B LST retrieval are still needed, especially in semi-arid regions where accurate land surface emissivity estimates are usually difficult to obtain. The objective of this paper is to develop and validate a single-channel algorithm by using different ancillary WVC data and single-channel thermal infrared data from the HJ-1B/IRS with a spatial resolution of 300 m in semi-arid regions in Heihe River Basin.

Section 2 describes the principle of the single-channel method developed for HJ-1B/IRS observations. Section 3 introduces the data used in the present study. Section 4 presents the comparison of the results with *in situ* measurements. Finally, the conclusions are presented in Section 5.

## 2. Methodology

When the sky is clear and a local thermodynamic equilibrium exists in the troposphere, the LST can be calculated from the Top Of Atmosphere (TOA) Brightness Temperature (BT) observations on the basis of the radiative transfer theory as follows Equation (1) [1]:

$$T_s = B_i^{-1} \left( \frac{B_i(T_{B_i}) - L_i \uparrow - (1 - \varepsilon_i) L_i \downarrow \cdot \tau_i}{\varepsilon_i \cdot \tau_i} \right) \quad (1)$$

where  $T_s$  is the LST (K),  $B_i$  is the Planck function ( $\text{W} \cdot \text{m}^{-2} \cdot \text{sr}^{-1} \cdot \mu\text{m}^{-1}$ ),  $i$  is the channel of the sensor,  $L_i \uparrow$  is the upwelling atmospheric radiance ( $\text{W} \cdot \text{m}^{-2} \cdot \text{sr}^{-1} \cdot \mu\text{m}^{-1}$ ),  $L_i \downarrow$  is the downwelling atmospheric irradiance divided by  $\pi$  ( $\text{W} \cdot \text{m}^{-2} \cdot \text{sr}^{-1} \cdot \mu\text{m}^{-1}$ ),  $\varepsilon_i$  is the land surface emissivity, and  $\tau_i$  is the total atmospheric transmittance along the path between the land surface and the satellite sensor.

The LSE can be estimated either based on the vegetation cover method [19], or on the classification-based method [15,20,21]. The effective emissivity of the land surface is calculated as follows Equation (2) [4]:

$$\varepsilon = \varepsilon_v FVC + \varepsilon_g (1 - FVC) \quad (2)$$

where  $\varepsilon_v$  is the vegetation emissivity,  $\varepsilon_g$  is the bare soil emissivity, and  $FVC$  is the fractional vegetation cover of a pixel and is calculated from the MODIS Normalized Difference Vegetation Index (NDVI) product (MOD13Q1) as follows Equation (3) [4]:

$$FVC = \left( \frac{NDVI - NDVI_s}{NDVI_v - NDVI_s} \right)^2 \quad (3)$$

where  $NDVI_v$  and  $NDVI_s$  are the  $NDVI$  values of fully covered vegetation and bare soil, respectively. In this paper,  $NDVI_v$  and  $NDVI_s$  are taken as the maximum and minimum values of the image, respectively.

Directional hemispherical reflectance values for different land cover types are provided by the Johns Hopkins University (JHU) spectral library, Advanced Spaceborne Thermal Emission Reflection Radiometer (ASTER) spectral library and MODIS spectral library (University of California, Santa Barbara (UCSB)) [22]. The channel land surface emissivities of HJ-1B/IRS are calculated by convolving the Spectral Response Function (SRF) with the spectral library emissivities as follows Equation (4) [15]:

$$\varepsilon = \frac{\int_{\lambda_1}^{\lambda_2} f(\lambda)\varepsilon(\lambda)d\lambda}{\int_{\lambda_1}^{\lambda_2} f(\lambda)d\lambda} \quad (4)$$

where  $f(\lambda)$  is the HJ-1B/IRS SRF (Figure 1),  $\lambda_1$  to  $\lambda_2$  is the wavenumber range in the SRF, and  $\lambda$  is the wavenumber.

Another essential procedure in the LST retrieval is to obtain the atmospheric parameters (including the atmospheric transmittance, atmospheric upward radiation and atmospheric downward radiation) for atmospheric correction. In the simulation using atmospheric transfer model MODTRAN 4.0 to acquire these parameters, Cloudless Land Atmosphere Radiosounding (CLAR), including 382 equally distributed global atmospheric profiles, is used in the method proposed by Li [15]. The relationship between the simulated atmospheric parameters (transmittance  $\tau$ , upwelling atmospheric radiance  $L^\uparrow$  and downwelling atmospheric radiance  $L^\downarrow$ ) and water vapor content ( $w$ ) are established by statistical regression from the simulation above.

However, Li [15] notes that the quadratic relationship between atmospheric parameters and WVC proposed by Jiménez-Muñoz and Sobrino [13] could lead major errors when the WVC is lower than 0.5 cm. Therefore, these parameters are derived as the cubic function of the WVC in our study as shown in Equations (5) to (7) [15]. The regression correlation coefficient (R) for each equation is 0.995, 0.990 and 0.992, respectively. Consequently, the atmospheric parameters could also be obtained with WVC when detailed relatively high accuracy atmospheric profiles are not available.

$$\tau = 0.98751 - 0.10396w - 0.01387w^2 + 0.00198w^3 \quad (5)$$

$$L^\uparrow = -0.00875 + 0.64736w + 0.20803w^2 - 0.02642w^3 \quad (6)$$

$$L^\downarrow = -0.02906 + 1.32128w + 0.14431w^2 - 0.02565w^3 \quad (7)$$

### 3. Data

#### 3.1. HJ-1B/IRS Data

The “Environmental and disaster monitoring and forecasting with a small satellite constellation” [23] comprises two small optical satellites (HJ-1A and HJ-1B) that were launched in 2008. The sensor of HJ-1B/IRS consists of four bands, *i.e.*, Near Infrared band (NIR, 0.75–1.10 microns), Shortwave Infrared band (SWIR, 1.55–1.75 microns), Middlewave Infrared band (MWIR, 3.50–3.90 microns) and Longwave Infrared band (LWIR, 10.5–12.5 microns). The spatial resolution of the NIR, SWIR and MWIR bands is 150 m and that of the LWIR band is 300 m. HJ-1B/IRS can provide global coverage every two days, and the revisit frequency is between the values of the MODIS and Landsat TM frequencies. The SRF of LWIR of HJ-1B/IRS is shown in Figure 1. Although HJ-1B/CCD suffers from a lens anomaly due to sensor design and atmospheric conditions [24], no lens anomalies have been found in HJ-1B/IRS data yet.

The HJ-1B/IRS data used in this paper cover 13 cloud-free days in 2012: 19 and 30 June; 8, 23 and 27 July; 14, 15, 22, and 29 August; and 2, 6, 14 and 17 September. The results are then compared with the ground data.

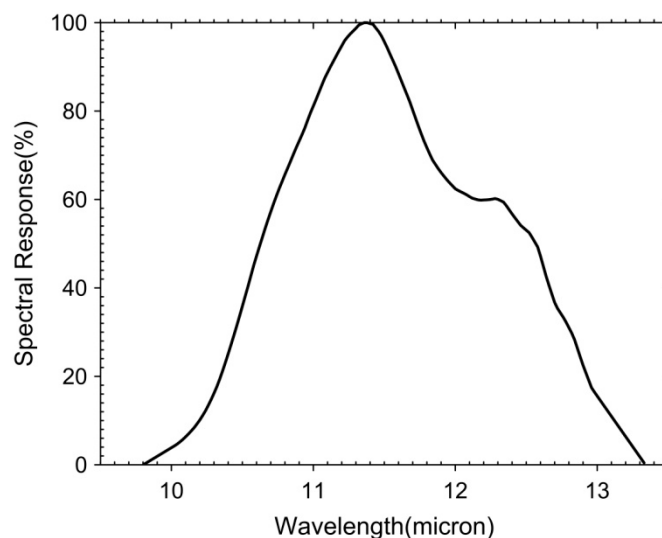


**Figure 1.** Spectral response function of HJ-1B/IRS in Longwave Infrared band (LWIR).

### 3.2. Ground Data

The ground data are from the Heihe Watershed Allied Telemetry Experimental Research (HiWATER) experiment in 2012. The experiment area is located in the middle reaches of the Heihe River Basin, a typical inland river basin with a semi-arid climate in Northwest China (Figure 2). The land surface is heterogeneous and is dominated by maize, vegetables, orchards, and residential areas. The spatial distribution of *in situ* Water Vapor Content measurements sites is also shown in Figure 2, including Wuxing Village (including Building 7 and Gouqu) and the Gaoya hydrological station. The details are shown on Section 3.3.2. Additional details can be found in Li *et al.* [25] and Liu *et al.* [26].

The *in situ* LST is derived from the land surface (Upwelling) Longwave Radiation (R<sub>lu</sub>) and atmospheric (Downwelling) Longwave Radiation (R<sub>ld</sub>), which were observed using four-component radiation measurements. For the radiometer intercomparison in HiWATER, the four-component radiation measurements exhibit good agreement. The average RMSE and Mean Relative Error (MRE) are 6.43 W·m<sup>-2</sup> and 0.62%, respectively, for R<sub>ld</sub> and 3.16 and -0.34%, respectively, for R<sub>lu</sub> [25,27]. The *in situ* measurements are stored in 10-min intervals, and the cloud-free measurements concurrent with the satellite overpasses (approximately 3:40 UTC, 11:40 Beijing Time both for HJ-1B and MODIS) are used for comparison with the retrieved LST.

Because of the large spatial variations, daytime *in situ* measurement data used in previous validation studies are scarce [2,28,29]. Although the spatial and temporal variability of the LST is smaller at nighttime, satellite-derived LST products should also be validated during the daytime because the LST data are mostly required during the day, e.g., for monitoring surface heat fluxes [30]. For these reasons, only the daytime values at the homogeneous sites (14 maize sites, 1 vegetable site, and 1 orchard site) were used in this study.

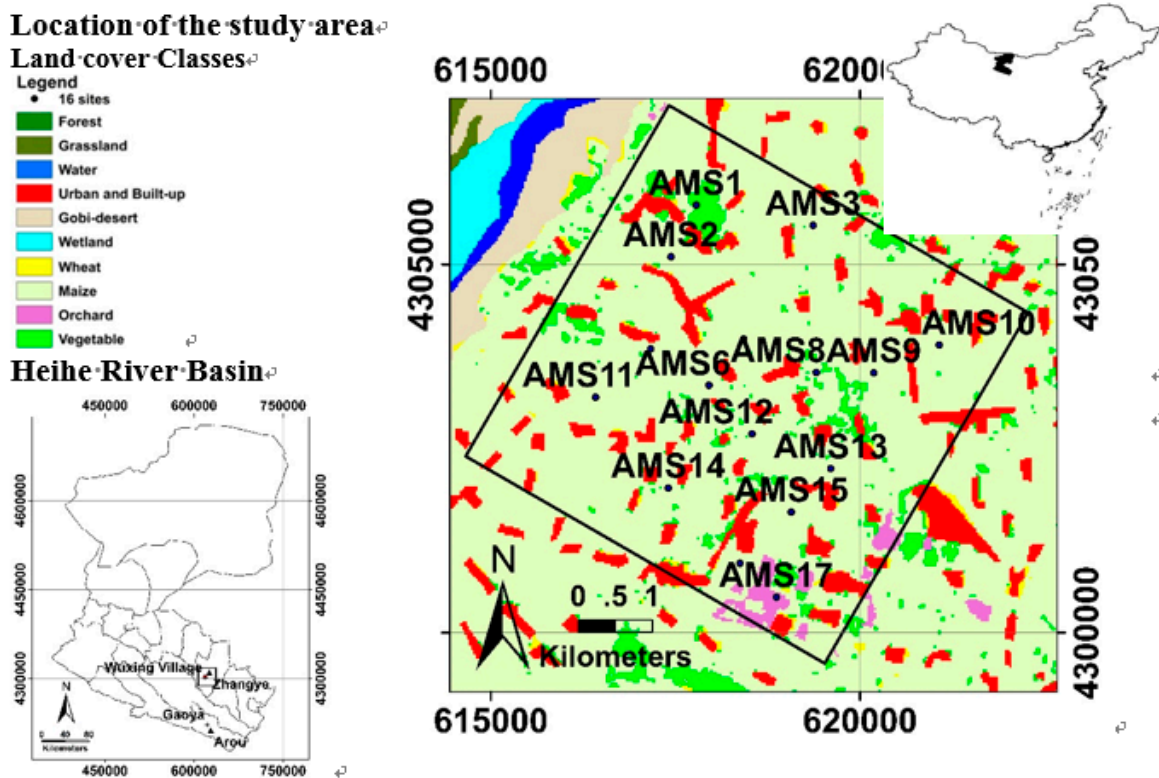


**Figure 2.** Location of the study area and distribution of the ground sites (including *in situ* LST measurements sites and WVC sites) used in this study. The location of the HiWATER-MUSOEXE area is indicated with the small red quadrangle (in the left image) and a solid black quadrangle (in the right image). The black square in the left image is the Heihe Matrix study area, which will be fully analyzed in the LST spatial distribution analyses.

### 3.3. MODIS Data and In Situ Water Vapor Content Data

#### 3.3.1. MODIS Data

MODIS, which is on board the Terra and Aqua satellites, has 36 spectral channels ranging from 0.405 to 14.385  $\mu\text{m}$ . The MODIS data products used in this study are given in Table 1 and, are downloaded from “Reverb”, a next generation metadata and service discovery tool [31]. It is worth noting that the MOD05 product is affected by the MODIS band 5 stripe noise. In this study, the noise is removed using median filtering with a  $9 \times 9$  pixel filter kernel. Moreover, the International Geosphere-Biosphere Program (IGBP) global vegetation classification from the land cover product MCD12Q1 is used.

**Table 1.** Specifications of the MODIS products used in this study.

Product Name	Spatial Resolution	Temporal Resolution	Name of Datasets and Usage
MOD03	1 km	Daily	Geolocation/Input
MOD05	1 km	Daily	WVC/Input
MOD11A1	1 km	Daily	LST/Validation
MOD13Q1	250 m	16 days	NDVI/Input
MCD12Q1	500 m	Yearly	Land cover types/Input

### 3.3.2. *In Situ* Water Vapor Content WVC Data

The *in situ* automatic sun tracking photometer CE318, which is provided by HiWATER from 19 June to 15 September 2012, includes two detectors that cover the entire spectrum from 340 to 1640 nm with eight bands. The detectors determine atmospheric parameters, such as aerosols and WVC (retrieved from the measurements at 936 nm). Other than the ground data, only 26 cloud-free samples of the CE318 data were acquired in this study. These data are obtained at the three sites in Zhangye and one site in Arou; these areas are shown in Figure 2. In Zhangye, the sites include Wuxing Village (Building 7), Wuxing Village (Gouqu) and the Gaoya hydrological station. It is worth noting that the CE318 data acquired at Building 7 and at Gouqu are from different days. As shown in Table 2, the data on June 19 are obtained at Building 7 and the other data are obtained at Gouqu.

**Table 2.** Comparison between MOD05-based LST, CE318-based LST and *in situ* LST at HiWATER AMS 5 in Wuxing Village.

Date (Month/Day)	MOD05-WVC (cm)	CE318-WVC (cm)	MOD05-Based- LST (K)	CE318-Based- LST (K)	<i>In Situ</i> -LST (K)
06/19	1.86	1.48	306.4	305.56	301.44
06/30	2.45	2.29	306.1	305.31	298.64
07/08	2.18	1.78	300	299.62	298.74
08/14	3.07	No data	295.3	No data	298.60
08/15	3.11	2.7	299.25	298.58	299.04
08/22	1.65	No data	299.8	No data	297.20
09/02	1.22	1.03	293.9	293.78	292.42
09/14	0.6	0.55	297.25	297.17	295.91
RMSE	0.12 cm		1.27 K	1.35 K	
R <sup>2</sup>	0.98		0.53	0.71	

## 4. Results and Discussion

### 4.1. Comparisons between MOD05 and *In Situ* Measurements of Water Vapor Content

The determination of atmospheric WVC is of vital importance in the retrieval of LST from satellite data. Although the usage of *in situ* WVC measurements can provide more accurate results than other satellite-based WVC data, the *in situ* WVC measurements are acquired for many reasons, such as human resources, time and other irresistible things. Therefore, the satellite-based WVC data are more economic and flexible. In this paper, the performance of the WVC from MODIS (MOD05), which are used for the HJ-1B/IRS atmospheric correction, is first assessed with the WVC from the *in situ* automatic sun-tracking photometer CE318 (referred to CE318-WVC).

The results from the cloud-free observations (Figure 3a) demonstrate that the values of the RMSE, MRE, and the determinant coefficient R<sup>2</sup> between the MOD05-WVC and CE318-WVC are 0.34 cm, 18%, and 0.93, respectively. Figure 3b clearly shows that the MOD05-WVC is slightly overestimated compared with the *in situ* CE318-WVC. When the WVC is approximately less than 1.5 cm (which usually occurs in semi-arid area), the WVC differences between the MOD05 product and the CE318

data are lower than 0.4 cm, which is acceptable in the LST retrievals. This result makes MOD05-WVC data reasonable for LST estimation in semi-arid area of the Heihe River Basin.

Among all the CE318 sites, Wuxing Village (Figure 2) provides the relatively complete observations: both CE318 data and *in situ* LST data are obtained here, and more cloud-free days occur. In this study, Table 2 presents the retrieved LST using the two WVC datasets for a maize site (AMS 5) in Wuxing Village. The largest LST difference between the MOD05-based LST and CE318-based LST appeared on June 19 as 0.84 K (with a WVC difference of 0.38 cm). The large error may be caused by the different atmospheric conditions at Building 7. The RMSE and  $R^2$  between the MOD05-WVC and CE318-WVC in Wuxing Village are 0.12 cm and 0.98, respectively. Meanwhile, the RMSE and  $R^2$  between the MOD05-based LST and *in situ* LST are 1.27 K and 0.53, respectively, and those between the CE318-based LST and *in situ* LST are 1.35 K and 0.71, respectively. The results demonstrate that use of the MOD05 product ensures a LST retrieval accuracy that is comparable to that produced when using the CE318 data.

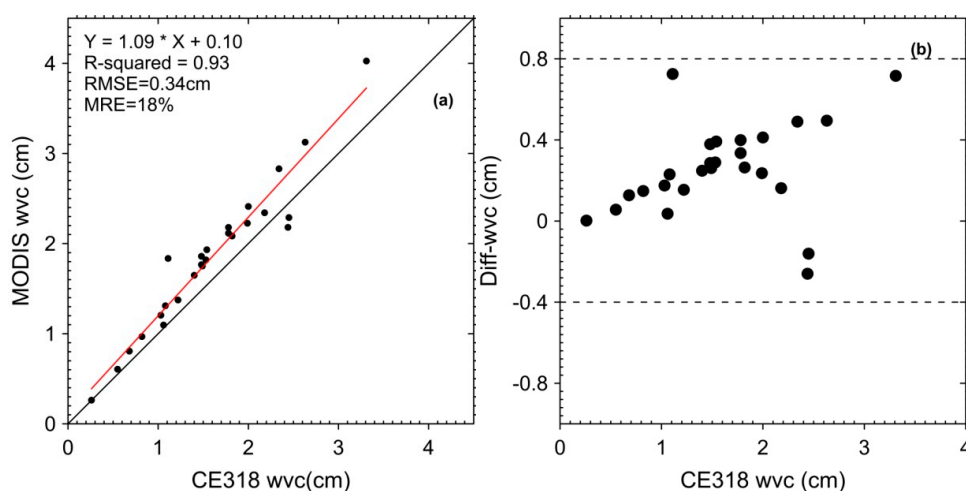


**Figure 3.** Scatter plots of (a) the MOD05-WVC and *in situ* CE318-WVC for cloud-free observations; (b) the difference between the MOD05-WVC and *in situ* CE318-WVC compared with the CE318-WVC at the HiWATER sites from 19 June to 15 September 2012. The number of valid samples is 26.

#### 4.2. HiWATER-MUSOEXE Results

Statistics of the comparisons between the HJ-1B/IRS LST, MODIS 1 km LST, and *in situ* AMS measurements for each of the HiWATER sites shown in Figure 2 are summarized in Table 3. Although there are fewer days with HJ-1B/IRS data than with MODIS data, both comparisons with *in situ* data yield similar results: the HJ-1B/IRS standard deviation (STD), RMSE, and linear correlation coefficient (R) values of HJ-1B/IRS vs. AMS are 2.45 K, 2.78 K, and 0.67 (with 204 samples), respectively, whereas those for the MODIS 1 km LST values are 4.07 K, 2.98 K, and 0.79 (with 886 samples), respectively.

A single Taylor [32] diagram is shown in Figure 4 to summarize multiple aspects of the method performance. The labels are assigned to six cases of the available data listed in Table 3. The position of each label on the plot quantifies how closely the estimation matches the *in situ* measurements. The RMSE (blue dotted semi-circle) between the estimated and *in situ* measurements is the difference from the “observed” values, which are defined as the *in situ* measurement STDs. The labels with a small

distance to the “observed” points (*i.e.*, smaller values of “observed” contours) correspond to the estimates that agree well with the *in situ* measurements. Most of these estimates have relatively high correlations and low RMSEs. The estimates that lie on or near the dashed arc have the correct STD. In Figure 4, it can be observed that label “a” (vegetables, HJ-1B/IRS) generally agrees better with the *in situ* measurements and exhibits lower RMSE and higher correlation. For the other labels (maize and orchards), the results are not as good, as the RMSEs are larger than 1.5 K (outside the dotted semi-circle of 1.50) and the correlations are lower than 0.9 (outside the green line of 0.9).

**Table 3.** Comparison of the HJ-1B/IRS and MODIS 1 km LST algorithm performance at the HiWATER sites (from June to September 2012).

Cropland	Product	Label (in Figure 4)	STD (K)	RMSE (K)	R	N (Samples)
Vegetable	HJ1B/IRS	a	3.40	1.42	0.94	12
	MODIS	A	3.61	2.32	0.85	53
Maize	HJ1B/IRS	b	2.58	2.83	0.67	180
	MODIS	B	4.06	3.01	0.79	778
Orchard	HJ1B/IRS	c	2.61	2.87	0.69	12
	MODIS	C	3.51	3.12	0.79	55

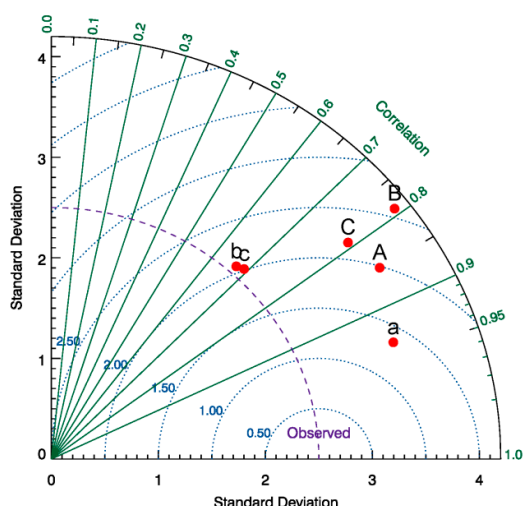


**Figure 4.** Taylor diagram that describes the performance of the LST retrieval from HJ-1B/IRS and MODIS over the HiWATER experiment sites in 2012.

The vegetable site (AMS 1, labeled “a” in Figure 4) is a relatively flat area with an elevation of 1552.75 m. Figure 5a indicates good agreement between the site observations and the satellite estimates at the vegetable site, which are also shown in Figure 4 and Table 3.

The 14 maize sites (AMS 2-AMS 3, AMS 5-AMS 16) are typical maize croplands in the HiWATER project. These sites are analyzed as a group in this study. The RMSE of 2.83 K in the maize area is acceptable due to the intercropping of certain croplands. The MODIS 1 km LST produces significant underestimations (the red ellipse in Figure 5b). These underestimations may partly be caused by the effect of clouds. It is difficult to efficiently exclude the clouds, especially in the partly cloudy pixels.

The orchard site (AMS 17) is planted with apple trees and intercropping maize. Unlike the vegetable and maize sites, the landscape at this site is heterogeneous. However, the results at the orchard site are

similar to those at the maize sites (Table 4 and Figure 4). This result is confirmed in Figure 5c. Figure 5c also shows that for the pixels of low temperatures, the estimation by HJ-1B/LST is much more consistent with the *in situ* values.

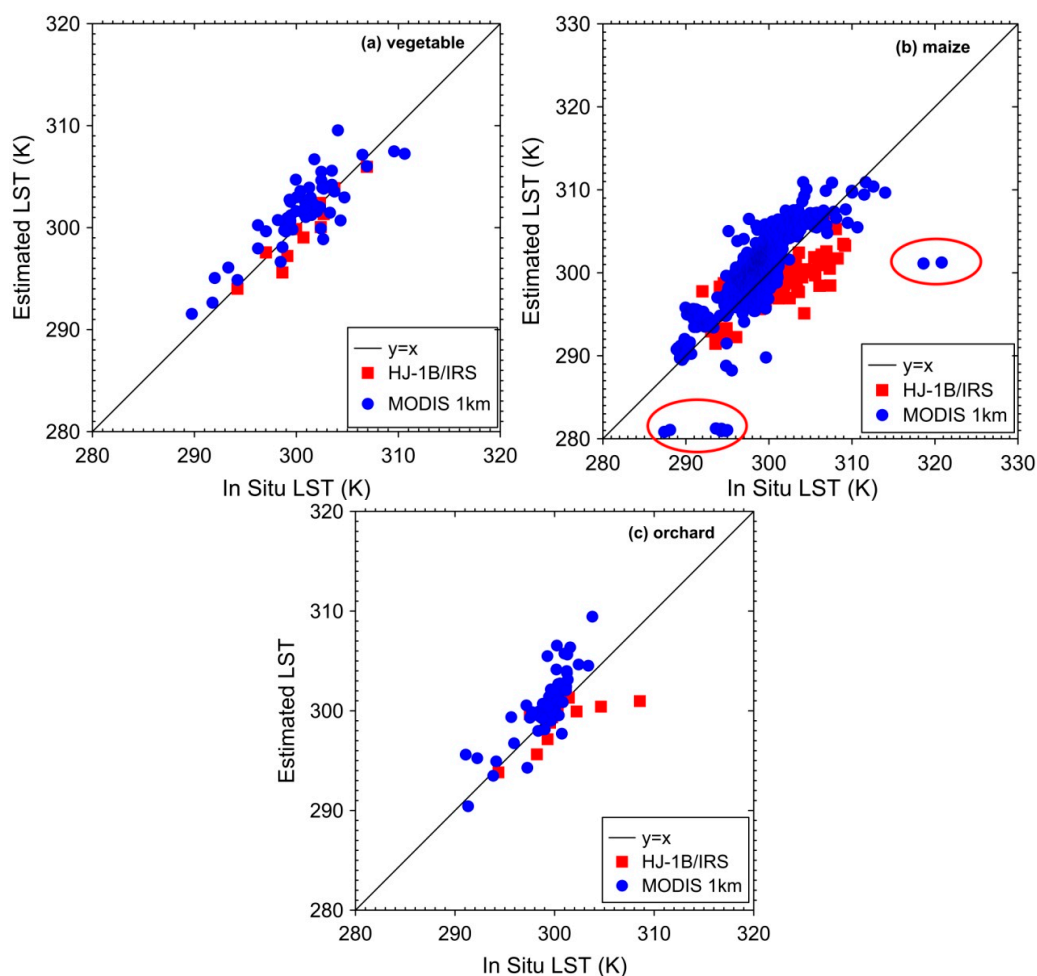


**Figure 5.** *In situ* LST vs. satellite-retrieved LST for three different land cover types: (a) vegetable (1 site), (b) maize (14 sites), and (c) orchard (1 site) from mid-June to mid-September 2012.

#### 4.3. Spatial Distribution

Because the purpose of this study is to retrieve the spatial distribution of LST that can be used for monitoring regional surface heat fluxes, it is important to assess the spatial distribution of the retrieved LST from the HJ-1B data. Figure 6 shows examples of the spatial distribution of the HJ-1B/IRS and MODIS 1 km LST. Both satellite images were acquired on 22 August 2012, and the MODIS 1 km LST data were resampled to 300 m. The HJ-1B/IRS data were acquired at approximately 3:50 UTC, (11:50 Beijing Time) while the MODIS data were acquired at 3:30 UTC (11:30 Beijing Time).

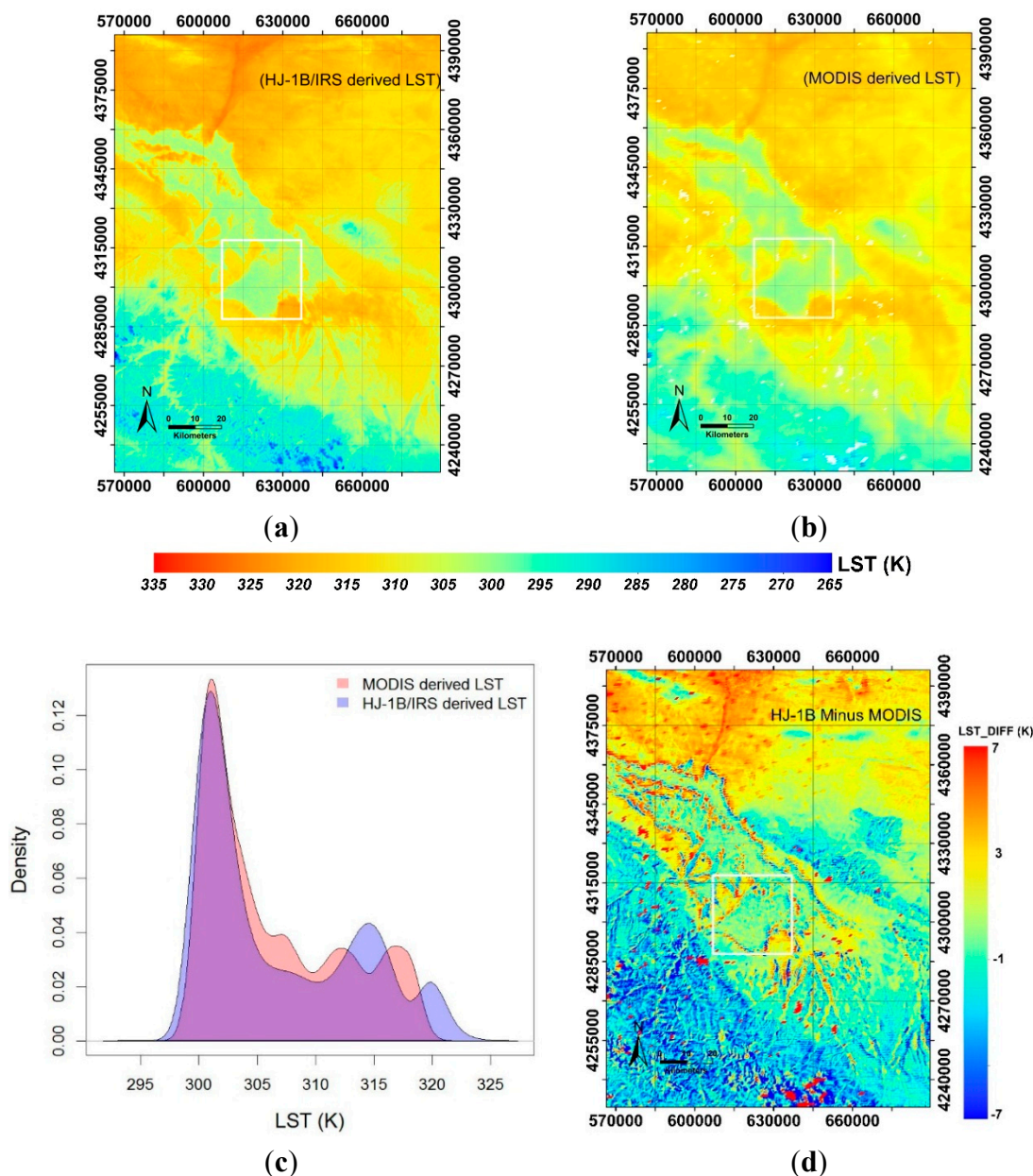


**Figure 6.** (a) The retrieved LST images with a 300 m resolution on 22 August 2012 (3:50 UTC, 11:50 Beijing Time); (b) the MODIS LST (3:30 UTC, 11:30 Beijing Time), where the white color is the MODIS cloud mask; (c) the density of the HJ-1B/IRS and MODIS derived LST for the 10000 pixels in the solid square; and (d) the difference between HJ-1B/IRS and MODIS derived LST.

Figure 7 shows the input parameters for the HJ-1B/IRS LST retrieval. The TOA radiance is between 4 and 11  $W \cdot m^{-2} \cdot sr^{-1} \cdot \mu m^{-1}$ . In the solid square (the irrigated oasis), the TOA radiance is approximately 9  $W \cdot m^{-2} \cdot sr^{-1} \cdot \mu m^{-1}$  when including the 16 AMS sites. The LSE is between 0.96 and 0.99, and the mean LSE is approximately 0.99. The WVC is approximately 1.5 cm. The WVC of the irrigated oasis is higher than that in the mountainous areas (the DEM shown in Figure 7d is higher than 4200 m) and desert (or sparsely vegetated in Figure 7e) because in the irrigated oasis, the irrigation provided more moisture. As mentioned (Figure 3b), when the WVC is approximately 1.5 cm, the WVC differences between the MOD05 product and the CE318 data are lower than 0.4 cm; thus, the LST differences between the

MOD05-based LST and CE318-based LST are less than 1 K. Figure 7d shows the Digital Elevation Data (DEM) obtained from the Shuttle Radar Topography Mission (SRTM) of the study area. The irrigated oasis is a nearly flat plain. Figure 7e shows the IGBP land cover type from MCD12Q1 product. These data are also the source data for LSE production. It should be mentioned that the spatial resolution of land cover data from MCD12Q1 is 500 m, which may have certain scaling effects on the LSE production that is used as a spatial resolution of 300 m in LST retrieval.

The spatial patterns of the retrieved HJ-1B/IRS LST over part of the middle stream and upstream regions of the Heihe River Basin generally agree well with the MODIS 1 km LST product (Figure 6). Generally, the HJ-1B/IRS LST product (Figure 6a) provides a more detailed texture for the study area (and other complex landscapes) than the MODIS product (Figure 6b) because of the higher spatial resolution of the HJ-1B data. Although the cloud mask (pixels in white color) in the MODIS 1 km product is not used in the HJ-1B/IRS product, the actual low temperatures could be discriminated from the image, such as the dark blue color in the image of Figure 6a. In the solid square, the mean LST is approximately 300 K for both images. Figure 6c shows the density comparison between HJ-1B/IRS and MODIS derived LST for the 10,000 pixels in the solid square. In Figure 6c, the cloud mask data (80 pixels in the solid square) in MODIS are excluded. To analyze the difference between HJ-1B/IRS and MODIS derived LST, the difference image between them is also obtained in Figure 6d. In the solid square and other flat and homogeneous places (cropland and grassland in Figure 7e), the differences between the two sensors derived LST are clearly shown to be within 1 K. The large differences occur both in mountainous areas and desert in the southwest and north of the image, respectively.

Figure 8 shows other comparison examples between the HJ-1B/IRS and MODIS derived LST in the growing season: (a) 16 May 2012 (*in situ* data were not available on this day in the former discussion); (b) 19 June 2012; and (c) 2 September 2012. The result with the obvious color changes indicates that the LST greatly changes during the growing season.

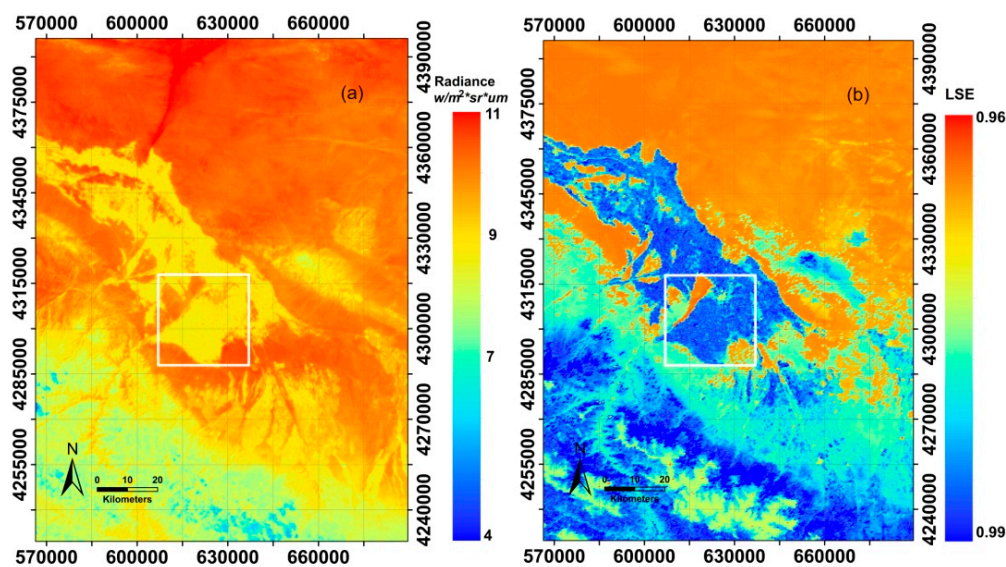
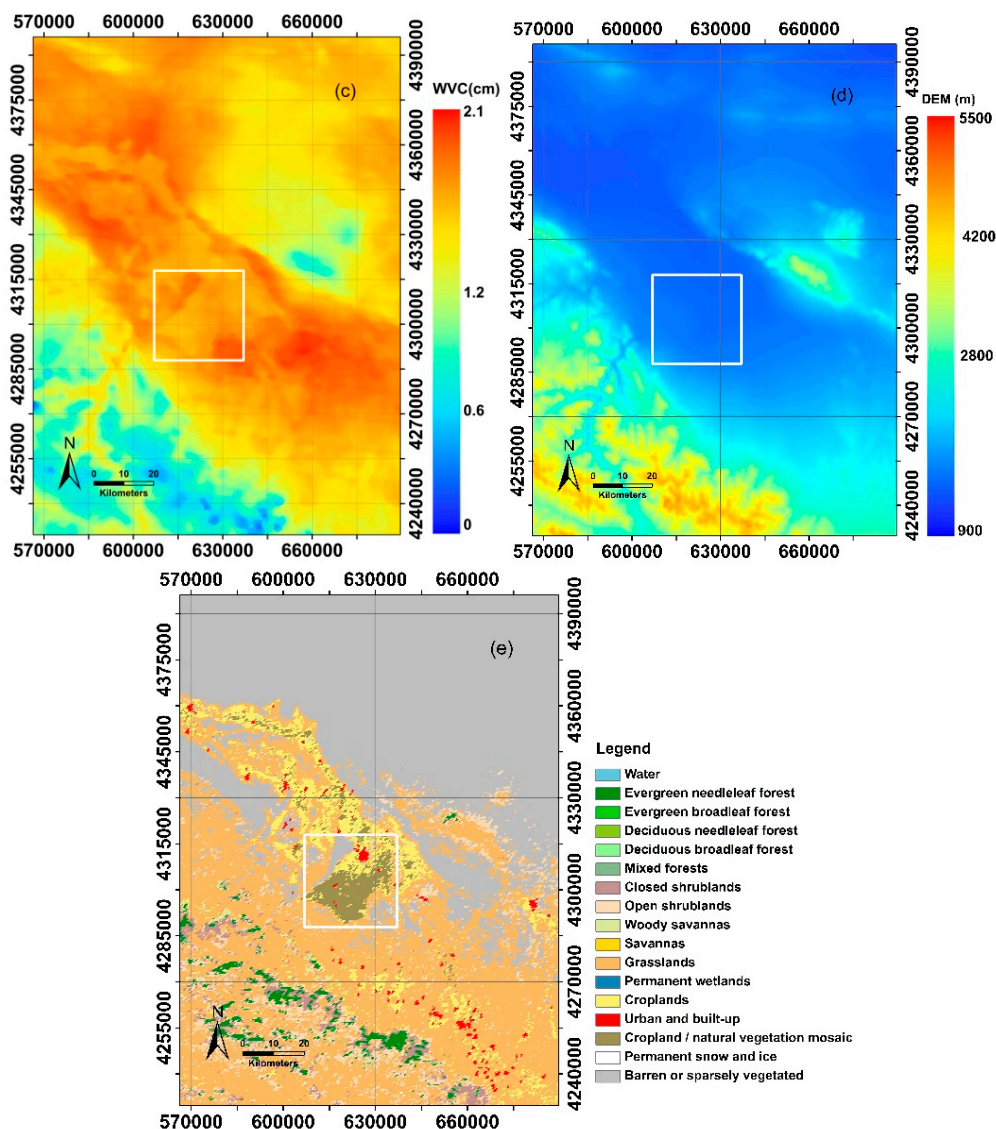


Figure 7. Cont.

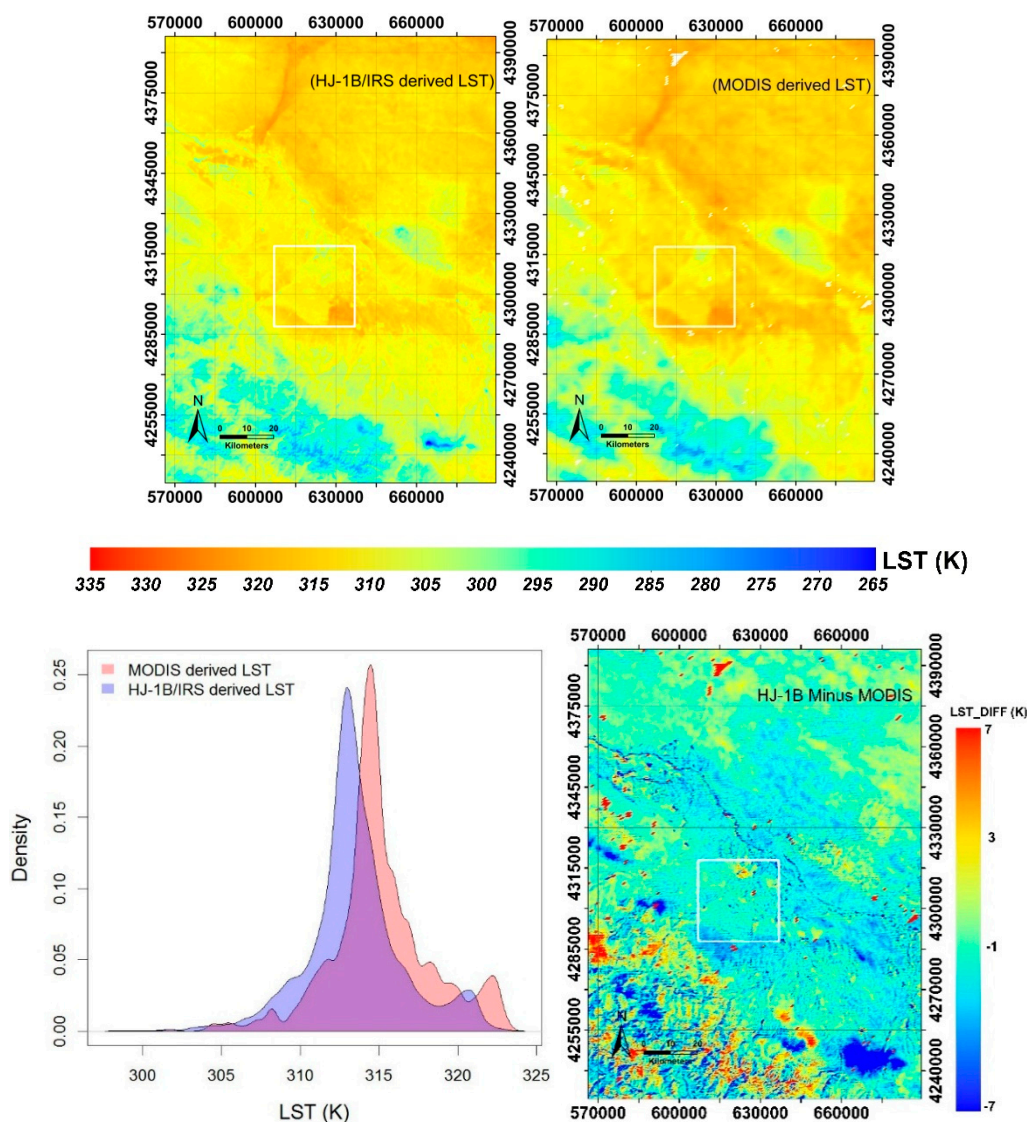


**Figure 7.** Input parameters for the HJ-1B/IRS LST retrieval at a 300 m resolution in the UTM projection (zone number 47N) for the study area; the location of the HiWATER Matrix is indicated by the white solid square on 22 August 2012. **(a)** HJ-1B/IRS TOA radiance; **(b)** estimated LSE; **(c)** MOD05 WVC data; **(d)** DEM obtained from Shuttle Radar Topography Mission (SRTM) and **(e)** MCD12Q1 land cover data.

On 16 May 2012, the plants were seeded in the Zhangye oasis (in the solid square) when the landscape was covered by sparse vegetation. Therefore, the LST image on this day is not as smooth as that of the fully covered vegetation days, such as 19 June 2012 and 2 September 2012. However, the difference between the results from two sensors is not as obvious. Furthermore, the large difference shown in Figure 8b may be heavily affected by the cloud on the retrieval images from two sensors.

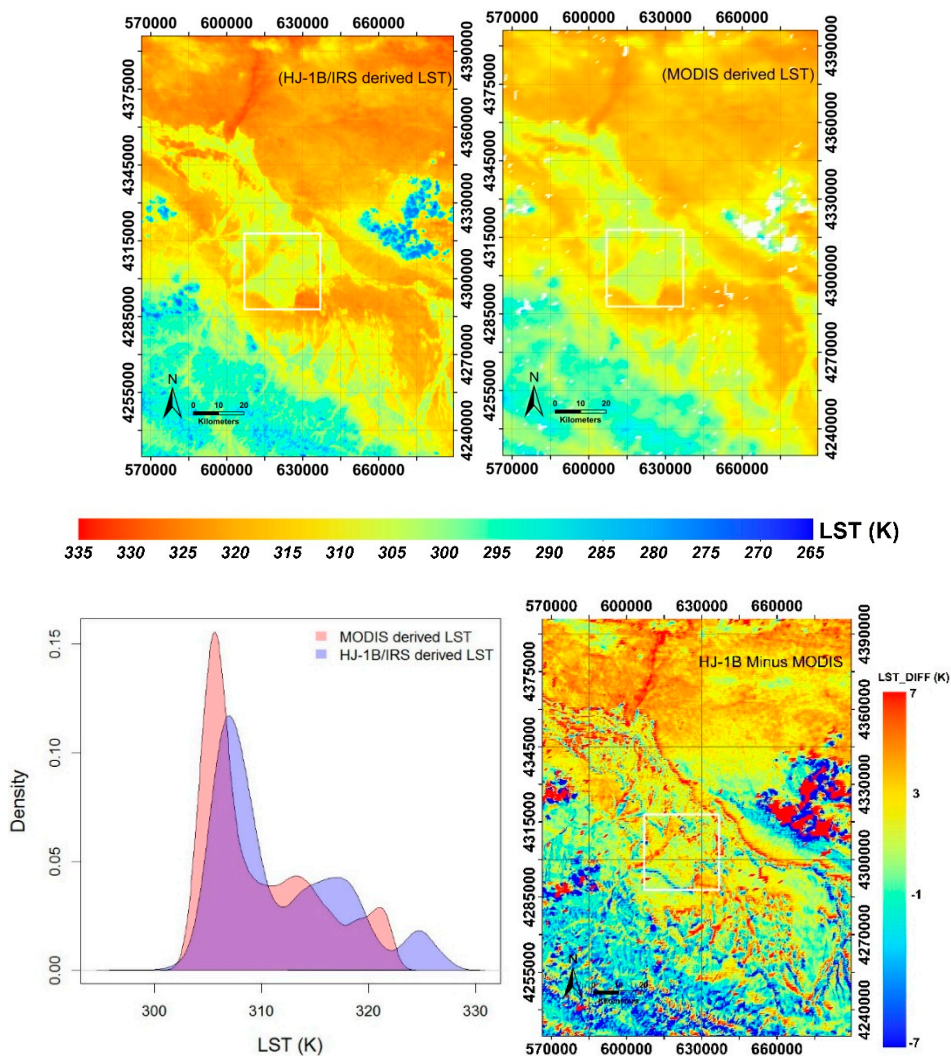
In the solid square, the view zenith angles (VZAs) of HJ-1B/IRS are all approximately 30 degrees. Meanwhile, the VZAs of MODIS vary from 10 degrees to 50 degrees in the same area. The VZA comparisons are shown in Table 4. Apparently, the minimum VZA differences between MODIS and HJ-1B/IRS occurred on 22 August 2012, in which the LST differences (Figure 7c) of MODIS and HJ-1B/IRS are also smaller than those on other days (Figure 8). Wan *et al.* [2] demonstrated that different

VZAs between different sources of measurements may result in different land surface emissivity values, as well as different LST retrieval results. In this study, although the VZA differences between HJ-1B and MODIS are expected to be small for fully covered croplands [17,33], the differences are still an important source for bias in the LST retrievals and impede the validation between different sensors. Additionally, low spectral information impedes accurate atmospheric correction of satellite data because single-channel sensors observe much less information on atmospheric conditions than multi-channel sensors. The proposed single-channel method in this paper is mainly suitable in semi-arid regions with low atmospheric WVC.



(a) 16 May 2012

Figure 8. Cont.



(b) 19 June 2012

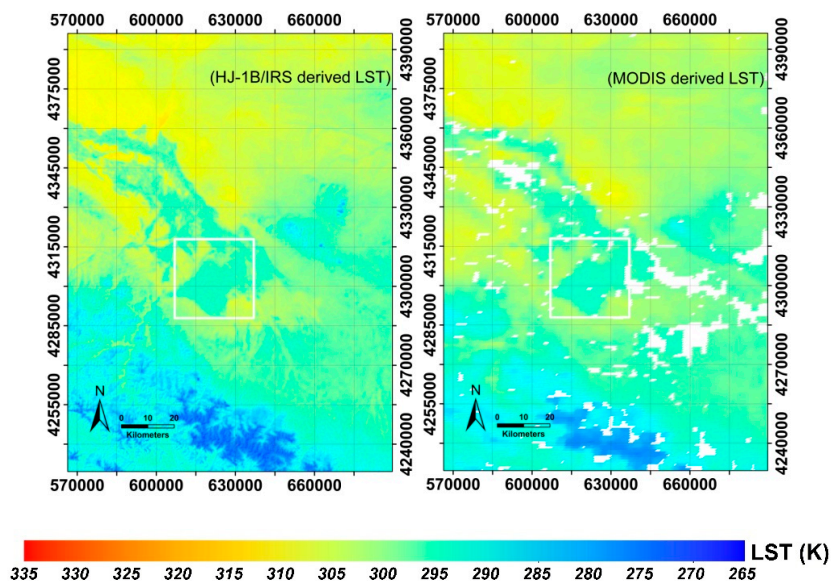
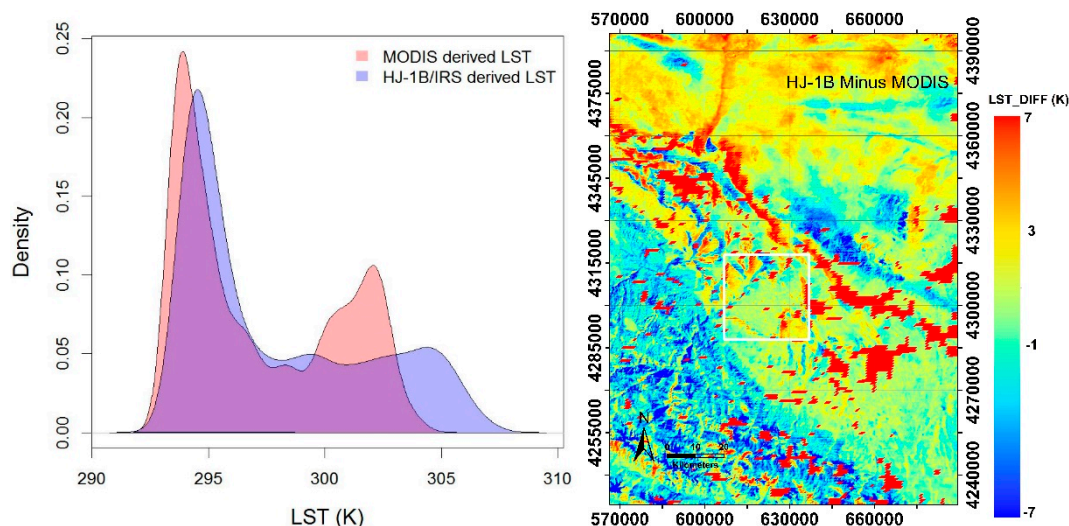


Figure 8. Cont.



(c) 2 September 2012

**Figure 8.** Similar to Figure 7, but for different days: (a) 16 May 2012; (b) 19 June 2012; and (c) 2 September 2012.

**Table 4.** Comparison of the HJ-1B/IRS and MODIS view zenith angles (VZAs) in the solid square from Figure 6 and Figure 8 in 2012.

Date (Month/Day)	View Zenith Angle (VZA, Degrees)	
	HJ-1B/IRS	MODIS
05/16	33	47
06/19	32	30
08/22	31	30
09/02	31	10

### 5. Conclusions

The reliable estimation of spatially distributed Land Surface Temperature (LST) is particularly crucial for monitoring regional surface heat fluxes. For the first time, a feasible single-channel algorithm has been developed to derive spatially distributed LST from the infrared sensor (IRS) onboard the Chinese “Environmental (HuanJing in Chinese) and disaster monitoring and forecasting with a small satellite constellation” (HJ-1B) with different ancillary data, *i.e.*, the MODIS water vapor content (WVC) product and *in situ* automatic sun tracking photometer CE318 data. The results show that the retrieved HJ-1B LST data, through use of the MOD05 WVC product, can achieve an accuracy comparable to that of the CE318 data for WVC. The largest LST difference between the MOD05-based LST and CE318-based LST was 0.84 K (associated with a WVC difference of 0.38 cm).

Additionally, the Standard Deviation (STD), Root Mean Square Error (RMSE), and correlation coefficient (R) of HJ-1B/IRS *vs.* the *in situ* measurements were 2.45 K, 2.78 K, and 0.67, whereas those for the MODIS 1 km LST *vs.* the *in situ* measurements were 4.07 K, 2.98 K, and 0.79, respectively.

The spatial pattern of the HJ-1B/LST over the study area in the Heihe River Basin generally agreed well with the MODIS 1 km LST product and contained more detailed spatial textures. In this study, although the view zenith angle (VZA) difference between HJ-1B and MODIS are expected to be small

for fully covered croplands, these differences are still important source of bias in LST retrievals and impede the validation between different sensors.

Low spectral information impedes the accurate atmospheric correction of satellite data because single-channel sensors observe much less information on atmospheric conditions than multi-channel sensors. The proposed single-channel method in this paper is mainly suitable for semi-arid regions with low atmospheric WVC.

To improve the validation process, future work should be dedicated to conducting careful and quantitative validations between different remotely sensed estimations and should eliminate the sensor attribute differences. Additionally, more surface sensors should be deployed to obtain *in situ* measurements during a field campaign.

### Acknowledgments

This work was jointly supported by the National Natural Science Foundation of China under grants 41101326 and 91025004 and project CAS/SAFEA Creative Research Teams (Grant nr. KZZD-EW-TZ-09). The authors would like to sincerely thank the China Center for Resources Satellite Data and Applications for providing the HJ-1B satellite data and the HiWATER program for providing the *in situ* measurements of the AMS and CE318 data.

### Author Contributions

Xiaoying Ouyang was responsible for the study and the write up of the manuscript. The co-authors provided supervision on manuscript construction and revision, and results analysis throughout the process.

### Conflicts of Interest

The authors declare no conflict of interest.

### References

1. Li, Z.-L.; Tang, B.-H.; Wu, H.; Ren, H.; Yan, G.; Wan, Z.; Trigo, I.F.; Sobrino, J.A. Satellite-derived land surface temperature: Current status and perspectives. *Remote Sens. Environ.* **2013**, *131*, 14–37.
2. Wan, Z.; Zhang, Q.; Li, Z.L. Quality assessment and validation of the MODIS global land surface temperature. *Int. J. Remote Sens.* **2004**, *25*, 261–274.
3. Duan, S.-B.; Li, Z.-L.; Tang, B.-H.; Wu, H.; Tang, R. Generation of a time-consistent land surface temperature product from MODIS data. *Remote Sens. Environ.* **2014**, *140*, 339–349.
4. Sobrino, J.A.; Jiménez-Muñoz, J.C.; Paolini, L. Land surface temperature retrieval from Landsat TM 5. *Remote Sens. Environ.* **2004**, *90*, 434–440.
5. Duan, S.-B.; Li, Z.-L.; Tang, B.-H.; Wu, H.; Tang, R. Direct estimation of land-surface diurnal temperature cycle model parameters from MSG-SEVIRI brightness temperatures under clear sky conditions. *Remote Sens. Environ.* **2014**, *150*, 34–43.
6. Roy, D.P.; Wulder, M.A.; Loveland, T.R. Landsat-8: Science and product vision for terrestrial global change research. *Remote Sens. Environ.* **2014**, *145*, 154–172.

7. Qin, Z.H.; Karnieli, A. A mono-window algorithm for retrieving land surface temperature from Landsat TM data and its application to the Israel–Egypt border region. *Int. J. Remote Sens.* **2001**, *22*, 3719–3746.
8. Li, H.; Liu, Q.H.; Du, Y.M.; Jiang, J.X.; Wang, H.S. Evaluation of the NCEP and MODIS atmospheric products for single channel land surface temperature retrieval with ground measurements: A case study of HJ-1B IRS data. *IEEE J. Stars.* **2013**, *6*, 1399–1408.
9. Duan, S.-B.; Li, Z.-L.; Wang, N.; Wu, H.; Tang, B.-H. Evaluation of six land-surface diurnal temperature cycle models using clear-sky *in situ* and satellite data. *Remote Sens. Environ.* **2012**, *124*, 15–25.
10. Ouyang, X.; Kang, G.; Zeng, F.; Qi, E.; Li, Z.L. Preliminary applications of a land surface temperature retrieval method to IASI and AIRS data. *Int. J. Remote Sens.* **2013**, *34*, 3128–3139.
11. Hu, C.; Tang, P. Automatic algorithm for relative radiometric normalization of data obtained from Landsat TM and HJ-1A/B charge-coupled device sensors. *J. Appl. Remote Sens.* **2012**, *6*, 063509.
12. Zhang, R.; Sun, R.; Du, J. Estimations of net primary productivity and evapotranspiration based on HJ-1A/B data in Jinggangshan City, China. *J. Mt. Sci.* **2013**, *10*, 777–789.
13. Jiménez-Muñoz, J.C.; Sobrino, J.A. A generalized single-channel method for retrieving land surface temperature from remote sensing data. *J. Geophys. Res.* **2003**, *108*, 1–9.
14. Sobrino, J.A.; Jiménez-Muñoz, J.C. Land surface temperature retrieval from thermal infrared data: An assessment in the context of the Surface Processes and Ecosystem Changes through Response Analysis (SPECTRA) mission. *J. Geophys. Res.* **2005**, *110*, doi:10.1029/2004JD005588.
15. Li, H. The Study of Algorithms for Land Surface Temperature Retrieval from HJ-1B/IRS and FY-3A/MERSI Data. Ph.D. Thesis, Institute of Remote Sensing Application, Chinese Academy of Science, Beijing, China, 2010. (In Chinese)
16. Zhao, L.; Yu, T.; Tian Q.; Gu X.; Li, J.; Wan, W. Error Analysis of the Land Surface Temperature Retrieval Using HJ-1B Thermal Infrared Remote Sensing Data. Available online: <http://europemc.org/abstract/MED/21322240> (accessed on 20 August 2014).
17. Coll, C.; Caselles, V.; Valor, E.; Raquel, N. Comparison between different sources of atmospheric profiles for land surface temperature retrieval from single channel thermal infrared data. *Remote Sens. Environ.* **2012**, *117*, 199–210.
18. Zhou, J.; Zhan, W.; Hu, D.; Zhao, X. Improvement of mono-window algorithm for retrieving land surface temperature from HJ-1B satellite data. *Chin. Geogr. Sci.* **2012**, *20*, 123–131.
19. Valor, E.; Caselles, V. Mapping land surface emissivity from NDVI: Application to European, African and South American areas. *Remote Sens. Environ.* **1996**, *57*, 167–184.
20. Snyder, W.; Wan, Z.; Zhang, Y.; Feng, Y.Z. Classification-based emissivity for land surface temperature measurement from space. *Int. J. Remote Sens.* **1998**, *19*, 2753–2774.
21. Li, H.; Liu, Q.H.; Jiang, J.X.; Wang, H.S.; Li, Q.; Sun, L. Land surface emissivity retrieval from HJ-1B satellite data using a combined method. In Proceedings of Geoscience and Remote Sensing Symposium (IGARSS), Vancouver, BC, Canada, 24–29 July 2011.
22. ASTER Spectral Library. <http://speclib.jpl.nasa.gov> (accessed on 26 June 2008).
23. Wang, Q.; Wu, C.Q.; Li Q.; Li, J.S. Chinese HJ-1A/B satellites and data characteristics. *Sci. Chin. Earth Sci.* **2010**, *53*, 51–57.

24. Li, Y.; Clarke, K.C. Image deblurring for satellite imagery using small-support-regularized deconvolution. *ISPRS J. Photogramm. Remote Sens.* **2013**, *85*, 148–155.
25. Li, X.; Cheng, G.D.; Liu, S.M.; Xiao, Q.; Ma, M.G.; Jin, R.; Che, T.; Liu, Q.H.; Wang, W.Z.; Qi, Y.; *et al.* Heihe Watershed Allied Telemetry Experimental Research (HiWATER): Scientific objectives and experimental design. *Bull. Am. Meteorol. Soc.* **2013**, *94*, 1145–1160.
26. Liu, S.M.; Xu, Z.W.; Wang, W.Z.; Bai, J.; Jia, Z.; Zhu, M.; Wang, J.M. A comparison of eddy-covariance and large aperture scintillometer measurements with respect to the energy balance closure problem. *Hydrol. Earth Syst. Sci.* **2011**, *15*, 1291–1306.
27. Xu, Z.; Liu, S.; Li, X.; Shi, S.; Wang, J.; Zhu, Z.; Xu, T.; Wang, W.; Ma, M. Intercomparison of surface energy flux measurement systems used during the HiWATER-MUSOEXE. *J. Geophys. Res. Atmos.* **2013**, *118*, 13140–13157.
28. Wan, Z.; Zhang, Y.; Zhang, Q.; Li, Z.L. Validation of the land-surface temperature products retrieved from Terra Moderate Resolution Imaging Spectroradiometer data. *Remote Sens. Environ.* **2002**, *83*, 163–180.
29. Coll, C.; Caselles, V.; Galve, J.M.; Valor, E.; Niclos, R.; Sanchez, J.M.; Rivas, R. Ground measurements for the validation of land surface temperatures derived from AATSR and MODIS data. *Remote Sens. Environ.* **2005**, *97*, 288–300.
30. Prata, A.J. Land Surface Temperature Measurement from Space: Validation of the AATSR Land Surface Temperature Product. Available online: <http://lst.nilu.no/Portals/73/Docs/Reports/Prata%202003%20-%20Land%20surface%20temperature%20measurement%20from%20space%20-%20Validation%20of%20the%20AATSR%20Land%20Surface%20Temperature%20Product.pdf> (accessed on 20 August 2014).
31. Reverb. Available online: <http://reverb.echo.nasa.gov> (accessed on 6 August 2013).
32. Taylor, K.E. Summarizing multiple aspects of model performance in a single diagram. *J. Geophys. Res.* **2001**, *106*, 7183–7192.
33. Lagouarde, J.P.; Kerr, Y.H.; Brunet, Y. An experimental study of angular effects on surface temperature for various plant canopies and bare soils. *Agr. Forest Meteorol.* **1995**, *77*, 167–190.